Research Square

Preprints are preliminary reports that have not undergone peer review.
They should not be considered conclusive, used to inform clinical practice,
or referenced by the media as validated information.

Enhanced oil removal from a real polymer production plant by cellulose nanocrystals - Serine incorporated polyethersulfone ultrafiltration membrane

Azar Asadi (azarasadi_88@yahoo.com)
Yasuj University: Yasouj University
Foad Gholami
Razi University of Kermanshah: Razi University
Ali Akbar Zinatizadeh
Razi University of Kermanshah: Razi University

Research Article

Keywords: Ultrafiltration, cellulose nanocrystals, oily wastewater, long-term performance

Posted Date: September 21st, 2021

DOI: https://doi.org/10.21203/rs.3.rs-793711/v2

License: This work is licensed under a Creative Commons Attribution 4.0 International License. Read Full License

Version of Record: A version of this preprint was published at Environmental Science and Pollution Research on January 15th, 2022. See the published version at https://doi.org/10.1007/s11356-021-18055-4.

Abstract

As discharging oily wastewater from industries to the environment is a potential threat for the aquatic ecosystem, in this research oil removal from a real case of Kermanshah polymer production plant wastewater was investigated. The focus of this study was on improving the oil rejection performance of polyethersulfone (PES) ultrafiltration membrane due to adding cellulose nanocrystals (CNC) and modified CNC with Serine amino acid (CNC-Ser) in PES mix matrix. From the results, the membranes embedded with CNC-Ser showed better performance in terms of water flux, flux recovery ratio and oil rejection (higher than 97%) compared to the modified membranes with CNC. The lowest water contact angle (41.370), the smoother surface and higher negative surface potential (-24 mv) was achieved for the optimum loading of CNC-Ser. Besides, long-term performance of the membranes with optimum loading of CNC and CNC-Ser were compared in both dead-end and cross-flow set-ups.

1. Introduction

With developing industrialization, the treatment of industrial wastewater has become a main concern in all over the world (Guan, Li, Zhu, & Xia, 2021). The treatment and disposal of oily wastewaters is a major challenge for some industries like petrochemical, food, and pharmaceutical. Petrochemical industry inevitably generates large volumes of oily wastewater over the chemical process for instance the production of high density polyethylene as a byproduct (Huang, Ras, & Tian, 2018; Li, Gao, Wang, Chen, & Yu, 2021). Therefore, petrochemical industry must separate oil from wastewater before releasing wastewater to environment. Also these days' seawater is being polluted by oil leakage and discharging effluents (Elshorafa, Saththasivam, Liu, & Ahzi, 2020). Various technology has been applied for treating oily wastewaters i.e. air flotation (Santos, Capponi, Ataíde, & Barrozo, 2021), ultrasonic irradiation (Sadatshojaie, Wood, Jokar, & Rahimpour, 2021), bioremediation (Mai et al., 2021), microwave irradiation (Garcia-Costa, Luengo, Zazo, & Casas, 2021) and pyrolysis (Singh, Singh, & Kumar, 2021). It has been proved that the mentioned methods are not qualified enough as a result of their disadvantaged like being costly, inefficient in low oil concentration ($\leq$ 100 ppm) and generate second pollutions in some cases (Pauzan, Abd Rahman, & Othman, 2021; Xinya Wang et al., 2020; Yan et al., 2019).

Membrane technology has been noticed by over recent decades resulted from its impressive separation even in low ranges of oil concentration, however, fouling phenomenon and needing to be cleaned frequently is a restriction for membrane technology (Eggensperger et al., 2020; Kamali, Costa, Aminabhavi, & Capela, 2019; Yusuf et al., 2020). Ultrafiltration has been used frequently for oil separation from oily wastewaters. In order to reduce the fouling phenomenon and increase the performance of ultrafiltration the polymeric membranes have been modified by different additives and fillers to obtain more hydrophilic membranes e.g., TiO_2 (Y.-X. Wang, Li, Yang, & Xu, 2019), carbon Nanotubes (CNT) (W. Wang et al., 2018), covalent organic framework (COF) (Fan, Gu, Meng, Knebel, & Caro, 2018), mesoporous (H. Liu et al., 2019), C_3N_4 (Shi et al., 2019), metal-organic framework (MOF) (F Gholami, Zinadini, Zinatizadeh, & Abbasi, 2018), and cellulose nanocrystals (Balcik-Canbolat & Van der Bruggen, 2020).

In 2019, Liu et al. reported mesoporous hybrid PAV/SiO_2 nanoparticle in PVDF membrane for simultaneous oil and heavy metals rejection. From the reported results, an acceptable heavy metal rejection beside of adequate anti-fouling ability and high water flux have been observed (H. Liu et al., 2019). Gholami and coworkers studied anti-fouling property and oily wastewater rejection by adding Zn based MOF (TMU-5) to PES polymer membrane (F Gholami et al., 2018). Due to hydrophilic nature of nanoparticles in membrane matrix, excellent hydrophilic and anti-fouling properties have been achieved. [21]. In another study, Lee et al. applied direct osmosis TFC membrane including poly [3-(N-2-methacryloylxyethyl-N, N-dimethyl)-ammonatopropanesulfonate] (PMAPS) for oil rejection from oily wastewater which high flux and low-fouling phenomenon, and 95% removal efficiency for oil emulation has been reported (Lee, Goh, Lau, Ong, & Ismail, 2019). Also, Zarghami and others used polymerization of dopamine on PES membrane which dopamine improved the water flux with good self-cleaning and anti-fouling properties (efficiency above 98%) (Zarghami, Mohammadi, & Sadrzadeh, 2019). Besides, ZnO microsphere/carbon nanotube as a filler in PES membrane has been also showed high rejecting, good flux and long-term stabling (Saththasivam, Wubulikasimu, Ogunbiyi, & Liu, 2019). In another research, ZNG-g-PVDF based membrane has been exhibited high anti-fouling quality and high oil rejection for very low concentration of oil pollution (13 ppm) (J. Zhang et al., 2018).

The application of nano-biomaterials as filler in polymer matrix has been noticed by researchers because of their favorite features like being cost-effective, biocompatible and nontoxic. Cellulose nanocrystals (CNCs) as renewable nano-scaled biomaterials have been applied in different researches to enhance and modify polymer characteristics due to its high hydrophilicity, good dispersion in water and polar solvents. Besides, the hydrophilic characteristics of CNC could be improved by conjugating with hydrophilic groups such as amino acids. Hence, amino acid with -COOH and $-NH_2$ groups provides superior hydrophilic nano-biomaterial compared to CNC alone, which has only -COOH group (Daraei, Ghaemi, & Ghari, 2017; Xuhong Wang et al., 2021).

From the literature, there are no any reports about using cellulose nanocrystals (CNC) modified with serine amino acids to improve hydrophilicity of PES membranes. CNC are derived from cellulose showed high surface area which have been applied for absorption and catalyst field. In spite of high stability and hydrophilicity of CNC, they have not been used broadly to improve the features of membranes for wastewater treatment. As a notice, it can be used to construct a novel membrane by the phase inversion method. In the current study, a nanocomposite UF membrane based on PES and CNC modified with serine amino acid including $-NH_2$ and -COOH functional groups is prepared via a phase inversion technique for purification of oily wastewaters. The CNC-Serine is firstly synthesized and characterized, and then embedded into the PES membrane. In order to identify membrane characteristics, contact angle, SEM, AFM, zeta potential and anti-fouling tests are used. It should be mentioned that the optimal membranes have been used to reject oil from Kermanshah polymer production plant wastewater.

2. Material And Methods

2.1. Materials

Polyethersulfone (PES) (MW= 58000 g.mol−1, ultrason E6020P) and dimethylacetamide (DMAc) as a solvent were purchased from BASF (Germany). Polyvinylpyrrolidone (PVP) (MW= 25000 g mol−1), and ethanol were purchased from Merck (Germany). All chemicals were used without further purification. The used milk powder was provided by commercial source (GUIGOZ Growth 3 Formula Milk Powder from 1 year to 3 years), and diesel oil was obtained from Oil Castrol Magnatec (10W-40). For membrane drying step, several filter papers of Whatman (1001-734 Grade 1, size: 46cmX100m) were used.

2.2. CNC modification

Serine and the carboxyl groups of CNC were counjugated by 1-Ethyl-3-(3-dimethylaminopropyl) carbodiimide (EDC)/ N-hydroxysuccinimide (NHS) coupling to synthesis amine functionalized CNC. Dried CNC was dispersed in ethanol by sonication for 45 min. EDC (54.3 mg, 0.4 mmol) and NHS (50.6 mg, 0.4 mmol) were added to the CNC solution (0.5 $g.ml^{-1}$, 0.5 g). Then, the serine was added to the CNC solution and stirred for 1 day at room temperature. The resulting CNC-Ser solution was centrifuged and washed in ethanol to remove unreacted serine (Fereiro et al., 2018).

2.3. Preparation of mixed matrix membrane

Phase inversion method has been applied for preparing Flat-sheet symmetric porous membranes modified with CNC based additives. The composition of the used different mixed solutions is shown in Table 1. An appropriate amount of additive was mixed with DMAc and sonicated (DT 102 H bandeling ultrasoni, Germany) for 25 min. Then, PVP and PES were added to the solution and mixed for 24 h (400 rpm). After obtaining homogeneous casting solution a film applicator and several neat glassy plates were utilized to fabricate membranes with thickness of 150 µm thickness. In next step, whole glass was immersed into distilled water (room temperature) to form the solid polymeric membranes. Then, the flat –sheet membranes were immersed into fresh distilled water for 24 h. In order to dry the obtained membranes, they were kept between two filter papers for another 24 h (Foad Gholami, Zinadini, & Zinatizadeh, 2020).

Table 1. The casting solution composition for membrane preparation

Membrane type	PES (wt.%)	PVP (wt.%)	DMAc (wt.%)	CNC-Ser (wt.%)
M1	18	1	81.0	-
M2	18	1	80.9	0.1[a]
M3	18	1	80.5	0.5[a]
M4	18	1	80.0	1.0[a]
M5	18	1	80.9	0.1[b]
M6	18	1	80.5	0.5[b]
M7	18	1	80.0	1.0[b]

a) CNC, b) CNC-Ser

2.4. Characterization of CNC-based membrane morphology

Scanning electron microscope (SEM, Philips-XL30, The Netherland) was applied with acceleration voltage of 20 kV. Small sample of membrane was frozen by liquid nitrogen and dried, then by sputtering, a thin layer of gold was coated on the membrane surface to make conduction. Atomic force microscopy (AFM) was used to study the surface of the prepared membranes. In this method specific area of the membrane sample (2×2 cm) was fixed on specimen holder, then a high-resolution microscope (Nanosurf® Mobile S scanning probe-optical microscope, Switzerland) physically scanned the level, three dimensionally (4×4 μm). The difference between peaks and valleys defined as surface roughness. Smoother surface has less difference in these parameters. The AFM images can be observed as Sa (average roughness), Sq (root of two data), and Sz (the average data between lowest valley and highest peak). The membrane water tendency was quantified by water contact angle (WCA) measurement. Less contact angle between membrane surface and water droplet indicates more hydrophilic nature. For this purpose, on the proper size of clean membrane, a small droplet of distilled water was injected (4 μL). After waiting for 10 seconds, to face with stable conditions, a digital microscope (Contact Anglemeter XCA-50) was captured the cross sectional images and the WCAs were calculated. More importantly to make the obtained results more reliable, 5 random places on the membrane surface were measured and average data was reported.

2.5. Porosity measurement of the prepared membranes

The membrane porosity was calculated based on gravimetric method. At first, 4 cm2 of all membranes was cut and weighted precisely, then submerged into distilled water for 24 h and finally it was weighted again. Based on Eq. 1, the membrane porosity was calculated:

$$\epsilon = \frac{\omega_1 - \omega_2}{\mathrm{A} \times \mathrm{L} \times \mathrm{dW}} \quad (1)$$

Which ω_1 and ω_2 are the wet and dry weight of membranes. A, L, and dW are effective surface, membrane thickness and water density (998 kg/m3), respectively.

Besides, mean pore radius (rm) was calculated according to Guerout–Elford–Ferry Eq. (2):

$$\mathrm{r_m} = \sqrt{\frac{(2.9 - 1.75\epsilon) \times 8\eta \mathrm{lQ}}{\epsilon \times \mathrm{A} \times \Delta \mathrm{P}}} \quad (2)$$

Where, η is the water viscosity (8.9×10 − 4 Pa s), Q is the volume of the permeate pure water per unit time (m3/s), and ΔP is the operating pressure (0.5 M Pa) (Samari, Zinadini, Zinatizadeh, Jafarzadeh, & Gholami, 2021).

The surface free energy (ΔGs) of the membranes was calculated using the Young Dupre equation (Eq. 3) (Hurwitz, Guillen, & Hoek, 2010).

$$-\Delta G_s = (1 + \cos\theta)\, \gamma_L \quad (3)$$

where θ is the water contact angle value and γL is the surface tension of water (72.8 mJ/m2).

2.6. Membrane setup and performance

A stainless steel dead-end setup with volume capacity of 150 ml and effective membrane surface of 12.56 cm2 was applied to evaluate membrane performance. The applied driving force to pass feed solution through the dead- end setup was the pressure of nitrogen gas (3 bar).

Also, to reduce feed polarization a stirrer was provided in setup. The weights of obtained samples passed through setup was determined by a digital balance and the pure water flux (PWF) was calculated based on Eq. 4:

$$J_{w.1} = \frac{M}{A\Delta t} \quad (4)$$

Where M, A, ΔT are permeating weight (kg), effective membrane area (m2), and filtration time (h), respectively (Foad Gholami, Zinadini, Zinatizadeh, & Samari, 2020).

Also, the long term performance of the optimum membranes in a cross-flow set- up with volumetric flow rate of 250 l/min and operating pressure of 3 bar was evaluated

2.7. Fouling effect

Resistance of the membranes was examined by passing milk powder solution (1000 ppm) through dead-end set up as fouling agent. At first, distilled water was passed through dead-end set up (60 min, 3 bar), in the second step, milk powder solution was filtered for 90 min, then the membrane was washed and immersed into distilled water (20 min), and finally, the distilled water was filtered again (60 min). After all, flux recovery ratio (FRR) and the membrane resistance are calculated according to Eq. 5 which FRR was considered as membrane resistivity against fouling:

$$FRR = \left(\frac{Jw2}{Jw1}\right) \times 100 \quad (5)$$

Where, JW1 and JW2 were PWF of the first step and second step, respectively. Different types of fouling including: total fouling ratio (Rt), reversible fouling ratio (Rr), and irreversible fouling ratio (Rir) were also calculated:

$$R_t(\%) = (1 - \frac{j_p}{j_{w.1}}) \times 100 \quad (6)$$

$$R_r(\%) = \left(\frac{j_{w.2} - j_p}{j_{w.1}}\right) \times 100 \quad (7)$$

$$R_{ir}(\%) = (\frac{j_{w.1} - j_{w.2}}{j_{w.1}}) \times 100 = R_t - R_r \quad (8)$$

2.8. Oil rejection and characteristics of Kermanshah polymer production plant wastewater

The simulated oily wastewater with 100, 300 and 500 ppm was utilized to investigate rejection performance and finally the long performance of the optimum membrane in removing oil from a real petroleum wastewater was examined in both dead-end and cross-flow set-up. In dead-end set-up, oil–water emulsion (diesel oil, SAF 40) has been provided by heating up the mixture at 50 ºC and stirring (400 rpm) for 100 min without emulsifier. Also, with applying stirrer and sonication the oil droplet size distribution was kept constant.

Also, Kermanshah polymer production plant wastewater, Kermanshah, Iran, as a real oily wastewater is used to evaluate the membrane performance in this study. The characteristics of the polymer production plant wastewater are as follow: COD of 500 mg/l, TSS of 395 mg/l, and pH of 5.5-7.

3. Results And Discussion

3.1. Characterization of CNC and CNC-Ser

For ensure to take place surface modification on CNC, FT-IR, SEM and zeta potential tests were performed. Figs 1a and b show FT-IR spectra for CNC and CNC-Ser, respectively. Also, he functional groups related to the observed bands have been specified. Based on the figs, the bands of NH2 (around 3500 cm-1), NH and COOH (around 1600 cm-1) were appeared in the FT-IR spectrum of CNC-Ser, however, they are not observed in the spectrum of CNC. This outcome is a firm evidence to modify CNC by serine (Chen et al., 2018; Zangeneh et al., 2019).

SEM images of CNC and CNC-Ser were illustrated in Figs 2a and b, respectively. From SEM images, the differences between the surface of CNC and CNC-Ser are obviously found out. The Figs showed that the surface of CNC was rougher rather than CNC-Seri. It should be noted that the surface of CNC was become slicker by inserting Serine amino acid on its surface (Azizi, 2020).

Besides, zeta potential of CNC and CNC-Ser was assessed as another evidence for surface modification which are shown in Figs 3a and b. Based on the Figs, the location of zeta potential peak and also the intensity of zeta potential peak were varied with surface modification of CNC. It is observed that zeta potential peak was shifted from -25 mv for CNC to -50 mv for CNC-Ser and also the intensity of zeta potential peak was altered from 4000 total counts for CNC to 6000 total counts for CNC-Ser (Mohan et al., 2021).

3.2. Membrane hydrophilicity

It is accepted that the presence of hydrophilic additives in membrane matrix caused a reduction in water contact angle (WCA) due to enhancing in membrane hydrophilicity. According to WCA results presented in Table 2, WCA of the bare membrane (M1) was decreased with addition of CNC and CNC-Se (M2-M7), verifying the effect of hydrophilic groups. In overall, the membranes embedded with CNC-Ser (M5-M7) showed lower WAC relative to the membranes embedded with CNC (M2-M5). This outcome is another prof for inserting Serine amino acid with NH2 and COOH groups on the surface of CNC which makes the surface more hydrophile. The lowest value of WCA was reported for the lowest loading of CNC-Ser (M5 with 0.1%)

as a result of the proper dispersion of the additive into the polymeric matrix. The WAC for the lowest loading of CNC and CNC-Ser was found to be 41.37 º and 63.52 º for M5 and M2, respectively, which this difference is a sign of the presence of hydrophilic functional groups of serine. It should be mention that an increase in the CNC-Ser loading (0.5, and 1.0 wt.%) resulted an increase in WCA and a reduction in the hydrophilicity of the membranes which could be explained by an increasing trend of the viscosity casting solution in higher loading of CNC-Ser. Moreover, the aggregation of nanostructures in higher loading could be another reason for decreasing homogeneity and increasing WCA besides the viscosity increscent (Samari, Zinadini, Zinatizadeh, Jafarzadeh, & Gholami, 2020).

In contrast to CNC-Ser, a decreasing trend of WCA is continued with increasing loading of CNC from 0.1-1%. Pure water flux (PWF) is another parameter to assess the presence of hydrophilic additives and porosity. According to presented data for PWF in Table 2, the membranes with CNC-Ser represented higher values of porosity and PWF for the membrane embedded with CNC-Ser (M5, 91.56 $kg/m^2.h$) compared to the membrane with incorporated CNC (M3, 70.42 $kg/m^2.h$). High hydrophilicity of M5 creates strong electrostatic interactions (e.g., hydrogen bonding) between the membrane surface functional groups (–COOH and –NH2) and water molecules caused the formation of a hydration layer on the surface of the membranes and also the channel walls in the membrane matrix (based on the Hagen–Poiseuille Flow equation). It should be notice that for both series of membranes with incorporated CNC and CNC-Ser, at higher loadings of additives agglomeration restricted porosity and PWF compared to lower loading of additives.

As an exception, PWF and porosity was not significantly decreased with increasing CNC loading from 0.1 to 0.5% as a result of the loaded porous nanoparticles, however, a reduction in PWF was observed from M5 (0.1%) to M6 (0.5%) (with CNC-Ser) due to occupying membrane pours and channels by serine functional groups.

Table 2. Surface parameter of the prepared membranes.

Membrane type	Porosity, %	Mean radius, nm	WCA, º	Surface free energy, mJ/m^2	PWF, $kg/m^2.h$
M1	47.45	9.26	78.65	87.13	33.38
M2	76.54	8.91	63.52	105.26	66.02
M3	79.42	8.88	59.03	110.26	70.42
M4	65.71	8.81	57.72	111.68	49.39
M5	88.23	9.11	41.37	127.43	91.56
M6	82.65	8.70	44.3	124.90	72.98
M7	72.31	8.93	46.25	123.14	59.92

3.3. Morphology analysis

Also, the tissue of the membranes was assessed by SEM cross-section analysis. According to Fig. 4 (SEM images), a dense top-layer for the modified membranes with higher loading of additives was notable. This is related to the viscosity of the casting solution that reduced the additives migration speed toward membrane surface during the phase inversion. As a report, the viscosity of the bare casting solution was increased from 366 (M1) to 412 for M5 and 489 for M7, indicating higher viscosity in higher loading of additives. It should be mentioned that top layer of the membranes at lower loading (M3 and M5) was more porous rather than the others (M4 and M7), causing an improvement in passing water through the membrane channels. Overall, the data of porosity were asserted by SEM cross-section images of the membranes. From Fig. 4, the presence of additives (CNC and CNC-Ser) creates obvious changes in the tissue of the membranes particularly at higher loading of additives resulted in more texture deformation (M4 and M7) (X. Liu et al., 2020).

Besides, to evaluate the roughness of the surface, AFM images of the bare and modified membranes are represented in Fig.5. The surface topography of the membrane's surface was investigated by mean roughness (Sa), root mean square of the Z data (Sq), and the difference between highest and lowest valleys (Sz) which were presented in Table 3. According to the Table, the values of Sa, Sq, Sz for modified membranes were lower than the bare membrane, indicating more smooth surface of the modified membranes. This result proved the presence of hydrophilic additives which enhanced the surface smoothness. M3 and M5 showed the least roughness for both membrane series with CNC and CNC-Ser, respectively, as a result of their good dispersions of additives in the polymeric matrix creating smoother surface with less wrinkled, while, the surface roughness increased at higher additive loading. Less roughness of M5 (Sa = 2.44 nm), compared to M3 (Sa = 2.99 nm) could be explained by more interactions between functional groups of CNC-Ser (NH2 and COOH) with the matrix of PES membrane exclusively over the phase inversion (Lee et al., 2019).

Table 3. The surface roughness of the unmodified and modified membrane.

Membrane	S_a (nm)	S_q (nm)	S_z (nm)
M1	18.13	22.63	104.57
M2	9.48	10.72	22.26
M3	2.99	3.83	24.70
M4	5.64	5.99	8.42
M5	2.42	2.97	6.58
M6	2.69	3.19	13.65
M7	2.42	3.26	13.68

3.4. Fouling behavior

Fouling behavior was evaluated by applying milk powder solution with concentration of 1000 mg/l as foulant solution. In this mean, three frequent steps were assessed including: distillated water-milk powder solution- distillated water. Fig. 6 illustrated the flux data over each step for all the membranes. The trends of changing flux for all membranes are similar, however, antifouling abilities and flux recoveries are different. From the Fig. the lowest flux for all three steps was observed for the bare membrane (M1) because of low porosity (47.45%, Table 2) and the hydrophobicity feature of bare PES membrane (WCA of 78.65º). In general, all the modified membranes showed better performance rather than the bare PES membrane, verifying the presence of hydrophilic additive. The highest flux over all three steps was obtained for M5 which based on Table 2 showed the lowest WCA and the highest porosity. The higher hydrophilicity of M5 enable the membrane to reject the foulant, provide satisfied flux, improve antifouling behavior and flux recovery. It should be noted that the higher performance of M5 is due to the presence of serine with polar functional groups (Vatanpour, Faghani, Keyikoglu, & Khataee, 2021).

Also, as zeta potential is an effective criterion for membrane performance in rejecting foulants and flux recovery, the surface charge of the bare membrane (M1) and the optimum membrane for each series (M3 for CNC series and M5 for modified CNC) at pH range of 4–8 was measured and presented in Fig.7. According to the Fig. all mentioned membrane displayed negative values of zeta potential (from –6.66 to –25.29 mV) and also an increase in PH value from 3 to 9 caused an increase in negative zeta potential (from –6.66 to –16.33 for M1, from –9.4 to –22.74 for M3, from –12.8 to –25.29 for M5). In each studied pH value, M5 exhibited the maximum surface negative charge compared to other membranes. It can be concluded that the negative charge density of CNC-Ser is improved by –COOH and $–NH_2$ functionalities on the top–layer rather than CNC, causing a high negative charge on the surface of M5. In point of fact, the results of surface zeta potential are in consist with the results of WCA presented in Table 2 and also is a good justification for obtaining the highest antifouling ability and flux recovery for M5 (Fig.6) (Hoseinpour, Ghaee, Vatanpour, & Ghaemi, 2018).

Flux recovery ratio (FRR) is a decent criterion to evaluate the performance of the prepared membranes besides PWF. Therefore, FRR was calculated for different prepared membranes and presented in Fig.8 (with milk powder solution as foulant). From the Fig. the lowest FRR was reported as 69.54% for the bare membrane, whereas, the membranes embedded with CNC and CNC-Ser showed an improvement in FRR. The highest values of FRR were achieved for M3 and M5. This result could be explained by surface zeta potential so that based on Fig. 7, M3 and M5 represented more negative surface charge, inhibiting cake layer formation. As a fact, at low loading additives the viscosity of the casting solution is low led to a fast migration of the additives over phase inversion, resulting more hydrophilicity, more surface free energy (Table 2), and more negative charge on the membrane surface. Moreover, FRR was reported as 93.41% and 83.34% for M5 and M3, respectively. The better performance of M5 could be explained by hydrogen bonding between-COOH and NH_2 groups of the modified CNC and H_2O molecules led to an increased membrane capability against cake layer formation on the membrane surface.

A reduced trend in FRR could be observed with increasing additive loadings, particularly for the unmodified CNC as a result of unpleasant dispersion and agglomeration in the membrane matrix. This reduction also could be related to surface roughness so that the higher surface roughness caused more foulant cake layer

formation on the membrane surface. From Table 4 and supplementary data 3, the surface of M3 and M5 was smoother rather than other membranes which is consistent with FRR results. Fouling took place for other membranes with higher surface roughness intensively, resulting lower FRR.

Moreover, in order to present more analysis about fouling phenomenon reversible and irreversible fouling (milk powder solution as foulant) were calculate for each membrane and presented in Fig. 8. From the Fig. the higher reversible fouling which is temporary and the lower irreversible fouling known as permanent fouling were obtained for the membranes embedded with CNC-Ser compared to the membranes with CNC. This outcome verified the better performance of CNC-Ser for improving the fouling characteristics of the bare membrane. As can be seen from the Fig., the bare membrane has the most irreversible fouling which caused a weak performance for applying it during several frequent filtrations. On the other hand, as observed in the Fig. over optimum loading of additives the reversible fouling of the bare membrane increased from 30.22 to 43.67 % and 53.22% for M3 and M5, respectively, while the irreversible fouling decreased notably from 30.45 to 16.65 % and 6.58% for M3 and M5, respectively (Foad Gholami, Zinadini, & Zinatizadeh, 2020; Vatanpour & Sanadgol, 2020).

3.6. Oil water removal

In this section, the performance of the prepared membranes in terms of oil rejection was investigated. In this mean three different feed concentrations (100, 300, 500 ppm oil) were examined for all membranes which the results are presented in Table 4. From the data of Table 4, the least FRR and flux values were reported for the bare membrane resulted from its high roughness, low antifouling ability, low porosity and its hydrophobic nature. The membrane embedded with CNC-Ser (modified additive) showed better performance in terms of flux and FRR compared to the membranes embedded with CNC in a good agreement with the data presented in Fig 5. Further improvement in the FRR and flux of the membranes with CNC-Ser, can be related to the presence of –COOH and $-NH_2$ groups in serine (M5) led to more surface charge, hydrophilicity, and less surface roughness. Besides, the performance of the prepared membranes for oil removal was assessed by COD removal as presented in Table 4. From COD removal results, the least efficiency for COD removal was reported for the bare membrane (M1) in all three levels of oil concentration. Similar to FRR and Flux data, the rejection performance of membranes embedded with CNC-Ser was higher rather than membranes modified with CNC in all three levels of oil concentration. The maximum COD removal was reported as 99% for M5 even for the least oil concentration (100 pm), indicating that M5 could be suggested to apply over the long-term filtration of oily wastewaters to provide a nearly stable high rejection and PWF (Foad Gholami, Zinadini, Zinatizadeh, et al., 2020).

Table 4. The oil separation results of the bare and modified in different oil concentrations.

	Flux, kg/m^2.h			FRR, %			COD removal, %		
	100 ppm	300 ppm	500 ppm	100 ppm	300 ppm	500 ppm	100 ppm	300 ppm	500 ppm
M1	17.05	20.46	21.49	74.32	76.36	75.87	58	65	72
M2	30.19	34.72	36.46	77..83	77.36	77.9	78	77	78
M3	36.03	41.44	45.17	88.34	89.89	90.24	90	90	93
M4	25.97	31.16	33.97	78.18	78.65	77.25	92	94	94
M5	47.82	58.34	62.76	98.41	98.99	99.2	99	99	99
M6	36.33	44.32	48.76	94.31	92.25	93.74	98	99	99
M7	29.19	35.03	38.54	92.41	91.89	90.32	97	97	98

Moreover, in order to have a good comparison with the literature some reported data was presented in Table 5. From Table 5, the rejection efficiency of the present research is similar to other studies, whereas, the amount of PWF and FRR are relatively high rather than the others. It should be noticed that the maximum PWF was 150 Kg/m^2.d reported from a study with TEG as an additive. Unlike the high amount of PWF, FRR value was relatively low about 45.3% for this research. In overall, cellulose nanocrystals – Serine showed a good performance for oil rejection with high PWF and FRR.

Table 5. Comparison of the prepared membranes' performance with other studies.

Polymer	Additive	Additive optimal concentration (wt%)	Operating pressure	Feed source	Rejection (%)	PWF $Kg/m^2.d$	FRR %	Ref
PSF	Zirconia/PEG	15	2 bar	Synthetic oil/ 80 ppm	99.16	-	-	(Y. Zhang, Cui, Du, Shan, & Wang, 2009)
PSF	PVP K40	5	1 bar	Synthetic oil/ 100 ppm	91	72	-	(Kumar, Nandi, Guria, & Mandal, 2017)
PES/15%	PVP/HMO	23.08	1 bar	Synthetic oil/ 100–1000 ppm	99	100	75	(Gohari et al., 2014)
PES/15%	PVP/HNT-HFO	23.08	1 bar	Synthetic oil/ 1000 ppm	99.7	80	-	(Ikhsan et al., 2018)
PES/15%	TEG	5	1.5 bar	Synthetic oil/3000 ppm	98.41	150	45.3	(Mokarizadeh & Raisi, 2021)
PES/18%	CuBTC	0.5	3 bar	Synthetic oil/4000 ppm	99	29.6	81	(Foad Gholami, Zinadini, & Zinatizadeh, 2020)
/PES/17%	UiO-66	0.5	3 bar	Synthetic oil/100-500 ppm	99	70	95.22	(Samari et al., 2020)
PES/17%	FSM-16	0.1	3 bar	Synthetic oil/100-500 ppm	99	61.95	99	(Samari et al., 2021)
PES/18%	**cellulose nanocrystals**	**0.1**	**3 bar**	**Real polymer petrochemical wastewater oil/100-500 ppm**	**99**	**105**	**99.2**	**This study**

3.7. Long-term performance

In this section, the long-term performance of the bare membrane, M3 and M5 for oil removal from Kermanshah polymer production plant wastewater in a dead-end set-up and a cross-flow set-up was investigated.

3.7.1. Dead-end set-up:

Flux data for long- term filtration of distillated water and Kermanshah polymer production plant wastewater alternately for M1 (bare membrane), M3 (optimal modified membrane with CNC), and M5 (optimal modified

membrane with CNC CNC-Ser) was presented in Fig.9a for 1100 min. It is obvious from the Fig. that the performance of the bare membrane is not satisfied and it could not be a proper case for long term performance as blocking took place for M1 after nearly three cycles. The main reason for this soon blocking of M1 is the hydrophobic nature of the bare PES membrane which adsorb oily components led to the formation of cake layer. Another reason is related to high surface roughness, causing trapping foulant agents. For modified membranes, seven cycles of distilled water were examined, and almost repeatable data were achieved. A gentle decreasing trend in water flux was observed for modified membranes particularly M5. The better performance of M5 is relate to the presence serine, offering more negative charge, antifouling ability, and permeation flux.

3.7.2. Cross-flow set-up:

Polymer production plant wastewater was passed through a cross-flow set-up for 600 min to evaluate the performance of M1, M3 and M5 and the flux data were presented in Fig.9b. Also, to evaluate flux recovery of the membranes after 600 min filtration of polymer production plant wastewater, distillated water was passed through set-up. It should be mentioned that oil was rejected over 97% for all three membranes, while, M1 presented the least water flux around 10 kg/m^2.h similar to dead-end setup, proving the inability of the bare ultrafiltration membrane to get stable oil rejection. Water flux for M3 and M5 was nearly stable around 40 and 85 kg/m^2.h, respectively. As M5 showed the highest water flux with acceptable stability and the highest flux recovery after 600 min, it could be suggested as a qualified ultrafiltration membrane to get a high stable rejection and water flux for treating Kermanshah polymer production plant wastewater.

4. Conclusion

In this study, water flux and antifouling characteristics of PES ultrafiltration membrane were improved with blending CNC and modified CNC with Serine amino acid (CNC-Ser). The presence CNC and CNC-Ser progressed the hydrophilicity, porosity, negative surface potential, water flux, and flux recovery ratio of the bare PES ultrafiltration membrane. However, CNC-Ser with –COOH and – NH_2 functional groups demonstrated more significant effect on the membrane properties and oil removal performance. The optimally modified membrane (0.1wt% of CNC-Ser) showed the least WCA (41.37 º), the highest PWF (91.56 kg/m^2.h) and FRR (93.41%), and great long-term filtration performance in both dead-end (1100 min) and cross-flow set-up (600min).

Declarations

- **Ethics approval and consent to participate**: Not applicable
- **Consent for publication**: The participant has consented to the submission of the case report to the journal.
- **Availability of data and materials**: All data generated or analysed during this study are included in this published article
- **Competing interests**: The authors declare that they have no competing interests

- **Funding:** Not applicable
- **Authors' contributions:**

All authors contributed to the study conception and design. Material preparation, data collection and analysis were performed by Foad Gholami and Azar Asadi. The first draft of the manuscript was written by Foad Gholami and Azar Asadi commented on previous versions of the manuscript. Ali Akbar Zinatizadeh read and approved the final manuscript.

- **Acknowledgements:**

The authors would like to acknowledge the central lab of Razi University for the support provided for this research work.

References

Azizi, A. (2020). Green Synthesis of Fe 3 O 4 Nanoparticles and Its Application in Preparation of Fe 3 O 4/Cellulose Magnetic Nanocomposite: A Suitable Proposal for Drug Delivery Systems. *Journal of Inorganic and Organometallic Polymers and Materials*, 1-10.

Balcik-Canbolat, C., & Van der Bruggen, B. (2020). Efficient removal of dyes from aqueous solution: the potential of cellulose nanocrystals to enhance PES nanocomposite membranes. *Cellulose, 27*(9), 5255-5266.

Chen, W., He, H., Zhu, H., Cheng, M., Li, Y., & Wang, S. (2018). Thermo-responsive cellulose-based material with switchable wettability for controllable oil/water separation. *Polymers, 10*(6), 592.

Daraei, P., Ghaemi, N., & Ghari, H. S. (2017). An ultra-antifouling polyethersulfone membrane embedded with cellulose nanocrystals for improved dye and salt removal from water. *Cellulose, 24*(2), 915-929.

Eggensperger, C. G., Giagnorio, M., Holland, M. C., Dobosz, K. M., Schiffman, J. D., Tiraferri, A., & Zodrow, K. R. (2020). Sustainable Living Filtration Membranes. *Environmental Science & Technology Letters, 7*(3), 213-218.

Elshorafa, R., Saththasivam, J., Liu, Z., & Ahzi, S. (2020). Efficient oil/saltwater separation using a highly permeable and fouling-resistant all-inorganic nanocomposite membrane. *Environmental Science and Pollution Research*, 1-10.

Fan, H., Gu, J., Meng, H., Knebel, A., & Caro, J. (2018). High-flux imine-linked covalent organic framework COF-LZU1 membranes on tubular alumina supports for highly selective dye separation by nanofiltration. *Angew. Chem., Int. Ed, 57*, 4083-4087.

Fereiro, J. A., Porat, G., Bendikov, T., Pecht, I., Sheves, M., & Cahen, D. (2018). Protein electronics: chemical modulation of contacts control energy level alignment in gold-azurin-gold junctions. *Journal of the American Chemical Society, 140*(41), 13317-13326.

Garcia-Costa, A. L., Luengo, A., Zazo, J. A., & Casas, J. A. (2021). Cutting oil-water emulsion wastewater treatment by microwave assisted catalytic wet peroxide oxidation. *Separation and Purification Technology, 257*, 117940.

Gholami, F., Zinadini, S., Zinatizadeh, A., & Abbasi, A. (2018). TMU-5 metal-organic frameworks (MOFs) as a novel nanofiller for flux increment and fouling mitigation in PES ultrafiltration membrane. *Separation and Purification Technology, 194*, 272-280.

Gholami, F., Zinadini, S., & Zinatizadeh, A. A. (2020). Preparation of high performance CuBTC/PES ultrafiltration membrane for oily wastewater separation; A good strategy for advanced separation. *Journal of Environmental Chemical Engineering, 8*(6), 104482.

Gholami, F., Zinadini, S., Zinatizadeh, A. A., & Samari, M. (2020). Preparation and Characterization of Antifouling Mixed Matrix Microfiltration Membranes Modified by Metal-Organic Frameworks for Usage in Membrane Bioreactor (MBR). *Environment and Water Engineering, 6*(2), 122-133.

Gohari, R. J., Halakoo, E., Lau, W., Kassim, M., Matsuura, T., & Ismail, A. (2014). Novel polyethersulfone (PES)/hydrous manganese dioxide (HMO) mixed matrix membranes with improved anti-fouling properties for oily wastewater treatment process. *RSC Advances, 4*(34), 17587-17596.

Guan, C., Li, Z., Zhu, L., & Xia, D. (2021). A superhydrophilic and high demulsification aramid nanofibers membrane with novel poly-pseudorotaxane structure for oil-in-water separation. *Separation and Purification Technology, 269*, 118715.

Hoseinpour, V., Ghaee, A., Vatanpour, V., & Ghaemi, N. (2018). Surface modification of PES membrane via aminolysis and immobilization of carboxymethylcellulose and sulphated carboxymethylcellulose for hemodialysis. *Carbohydrate Polymers, 188*, 37-47.

Huang, S., Ras, R. H., & Tian, X. (2018). Antifouling membranes for oily wastewater treatment: Interplay between wetting and membrane fouling. *Current opinion in colloid & interface science, 36*, 90-109.

Hurwitz, G., Guillen, G. R., & Hoek, E. M. (2010). Probing polyamide membrane surface charge, zeta potential, wettability, and hydrophilicity with contact angle measurements. *Journal of membrane science, 349*(1-2), 349-357.

Ikhsan, S. N. W., Yusof, N., Aziz, F., Misdan, N., Ismail, A. F., Lau, W.-J., . . . Hairom, N. H. H. (2018). Efficient separation of oily wastewater using polyethersulfone mixed matrix membrane incorporated with halloysite nanotube-hydrous ferric oxide nanoparticle. *Separation and Purification Technology, 199*, 161-169.

Kamali, M., Costa, M. E., Aminabhavi, T. M., & Capela, I. (2019). Sustainability of treatment technologies for industrial biowastes effluents. *Chemical Engineering Journal, 370*, 1511-1521.

Kumar, S., Nandi, B., Guria, C., & Mandal, A. (2017). Oil removal from produced water by ultrafiltration using polysulfone membrane. *Brazilian Journal of Chemical Engineering, 34*, 583-596.

Lee, W., Goh, P., Lau, W., Ong, C. S., & Ismail, A. (2019). Antifouling zwitterion embedded forward osmosis thin film composite membrane for highly concentrated oily wastewater treatment. *Separation and Purification Technology, 214*, 40-50.

Li, M., Gao, X., Wang, X., Chen, S., & Yu, J. (2021). Wettable and Flexible Silica Nanofiber/Bead-Based Membranes for Separation of Oily Wastewater. *ACS Applied Nano Materials, 4*(3), 2952-2962.

Liu, H., Yu, H., Yuan, X., Ding, W., Li, Y., & Wang, J. (2019). Amino-functionalized mesoporous PVA/SiO2 hybrids coated membrane for simultaneous removal of oils and water-soluble contaminants from emulsion. *Chemical Engineering Journal, 374*, 1394-1402.

Liu, X., Yuan, H., Wang, C., Zhang, S., Zhang, L., Liu, X., . . . Ching, C. (2020). A novel PVDF/PFSA-g-GO ultrafiltration membrane with enhanced permeation and antifouling performances. *Separation and Purification Technology, 233*, 116038.

Mai, C. T. N., Linh, N. V., Lich, N. Q., Ha, H. P., Van Quyen, D., Tang, D. Y. Y., & Show, P. L. (2021). Advanced materials for immobilization of purple phototrophic bacteria in bioremediation of oil-polluted wastewater. *Chemosphere, 278*, 130464.

Mohan, T., Chirayil, C. J., Nagaraj, C., Bračič, M., Steindorfer, T. A., Krupa, I., . . . Stana Kleinschek, K. (2021). Anticoagulant Activity of Cellulose Nanocrystals from Isora Plant Fibers Assembled on Cellulose and SiO2 Substrates via a Layer-by-Layer Approach. *Polymers, 13*(6), 939.

Mokarizadeh, H., & Raisi, A. (2021). Industrial wastewater treatment using PES UF membranes containing hydrophilic additives: Experimental and modeling of fouling mechanism. *Environmental Technology & Innovation*, 101701.

Pauzan, M. A. B., Abd Rahman, M., & Othman, M. H. D. (2021). Hydrocarbon Separation and Removal Using Membranes. In *Membrane Technology Enhancement for Environmental Protection and Sustainable Industrial Growth* (pp. 73-90): Springer.

Sadatshojaie, A., Wood, D. A., Jokar, S. M., & Rahimpour, M. R. (2021). Applying ultrasonic fields to separate water contained in medium-gravity crude oil emulsions and determining crude oil adhesion coefficients. *Ultrasonics Sonochemistry, 70*, 105303.

Samari, M., Zinadini, S., Zinatizadeh, A. A., Jafarzadeh, M., & Gholami, F. (2020). Designing of a novel polyethersulfone (PES) ultrafiltration (UF) membrane with thermal stability and high fouling resistance using melamine-modified zirconium-based metal-organic framework (UiO-66-NH2/MOF). *Separation and Purification Technology, 251*, 117010.

Samari, M., Zinadini, S., Zinatizadeh, A. A., Jafarzadeh, M., & Gholami, F. (2021). A new fouling resistance polyethersulfone ultrafiltration membrane embedded by metformin-modified FSM-16: Fabrication, characterization and performance evaluation in emulsified oil-water separation. *Journal of Environmental Chemical Engineering, 9*(4), 105386.

Santos, M. A., Capponi, F., Ataíde, C. H., & Barrozo, M. A. (2021). Wastewater treatment using DAF for process water reuse in apatite flotation. *Journal of cleaner production, 308*, 127285.

Saththasivam, J., Wubulikasimu, Y., Ogunbiyi, O., & Liu, Z. (2019). Fast and efficient separation of oil/saltwater emulsions with anti-fouling ZnO microsphere/carbon nanotube membranes. *Journal of Water Process Engineering, 32*, 100901.

Shi, Y., Huang, J., Zeng, G., Cheng, W., Hu, J., Shi, L., & Yi, K. (2019). Evaluation of self-cleaning performance of the modified g-C3N4 and GO based PVDF membrane toward oil-in-water separation under visible-light. *Chemosphere, 230*, 40-50.

Singh, B., Singh, S., & Kumar, P. (2021). In-depth analyses of kinetics, thermodynamics and solid reaction mechanism for pyrolysis of hazardous petroleum sludge based on isoconversional models for its energy potential. *Process Safety and Environmental Protection, 146*, 85-94.

Vatanpour, V., Faghani, S., Keyikoglu, R., & Khataee, A. (2021). Enhancing the permeability and antifouling properties of cellulose acetate ultrafiltration membrane by incorporation of ZnO@ graphitic carbon nitride nanocomposite. *Carbohydrate Polymers, 256*, 117413.

Vatanpour, V., & Sanadgol, A. (2020). Surface modification of reverse osmosis membranes by grafting of polyamidoamine dendrimer containing graphene oxide nanosheets for desalination improvement. *Desalination, 491*, 114442.

Wang, W., Zhu, L., Shan, B., Xie, C., Liu, C., Cui, F., & Li, G. (2018). Preparation and characterization of SLS-CNT/PES ultrafiltration membrane with antifouling and antibacterial properties. *Journal of membrane science, 548*, 459-469.

Wang, X., Feng, N., Shi, Z., Zhou, N., Lu, J., Huang, J., & Gan, L. (2021). Stimuli-responsive flexible membrane via co-assembling sodium alginate into assembly membranes of rod-like cellulose nanocrystals with an achiral array. *Carbohydrate Polymers, 262*, 117949.

Wang, X., Xiao, C., Liu, H., Chen, M., Xu, H., Luo, W., & Zhang, F. (2020). Robust functionalization of underwater superoleophobic PVDF-HFP tubular nanofiber membranes and applications for continuous dye degradation and oil/water separation. *Journal of membrane science, 596*, 117583.

Wang, Y.-X., Li, Y.-J., Yang, H., & Xu, Z.-L. (2019). Super-wetting, photoactive TiO2 coating on amino-silane modified PAN nanofiber membranes for high efficient oil-water emulsion separation application. *Journal of membrane science, 580*, 40-48.

Yan, L., Zhang, G., Zhang, L., Zhang, W., Gu, J., Huang, Y., . . . Chen, T. (2019). Robust construction of underwater superoleophobic CNTs/nanoparticles multifunctional hybrid membranes via interception effect for oily wastewater purification. *Journal of membrane science, 569*, 32-40.

Yusuf, A., Sodiq, A., Giwa, A., Eke, J., Pikuda, O., De Luca, G., . . . Chakraborty, S. (2020). A review of emerging trends in membrane science and technology for sustainable water treatment. *Journal of cleaner production*,

121867.

Zangeneh, H., Zinatizadeh, A. A., Zinadini, S., Feyzi, M., Rafiee, E., & Bahnemann, D. W. (2019). A novel L-Histidine (C, N) codoped-TiO2-CdS nanocomposite for efficient visible photo-degradation of recalcitrant compounds from wastewater. *Journal of hazardous materials, 369*, 384-397.

Zarghami, S., Mohammadi, T., & Sadrzadeh, M. (2019). Preparation, characterization and fouling analysis of in-air hydrophilic/underwater oleophobic bio-inspired polydopamine coated PES membranes for oily wastewater treatment. *Journal of membrane science, 582*, 402-413.

Zhang, J., Zhang, F., Wang, A., Lu, Y., Li, J., Zhu, Y., & Jin, J. (2018). Zwitterionic nanofibrous membranes with a superior antifouling property for gravity-driven crude oil-in-water emulsion separation. *Langmuir, 35*(5), 1682-1689.

Zhang, Y., Cui, P., Du, T., Shan, L., & Wang, Y. (2009). Development of a sulfated Y-doped nonstoichiometric zirconia/polysulfone composite membrane for treatment of wastewater containing oil. *Separation and Purification Technology, 70*(2), 153-159.

Supplemental Note

Supplementary Data not available with this version

Figures

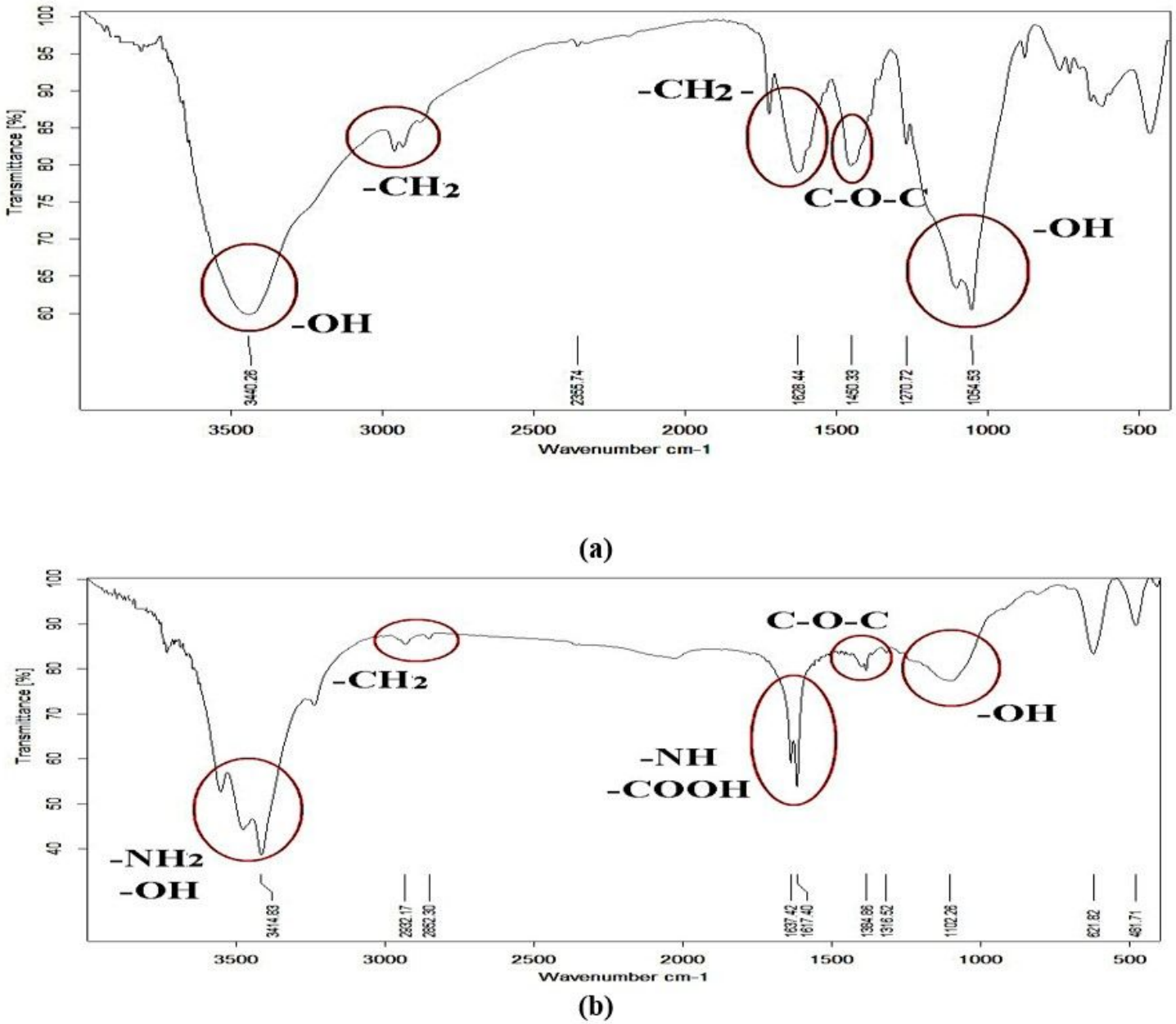

Figure 1

FT-IR spectra of CNC (a) and CNC-Ser (b).

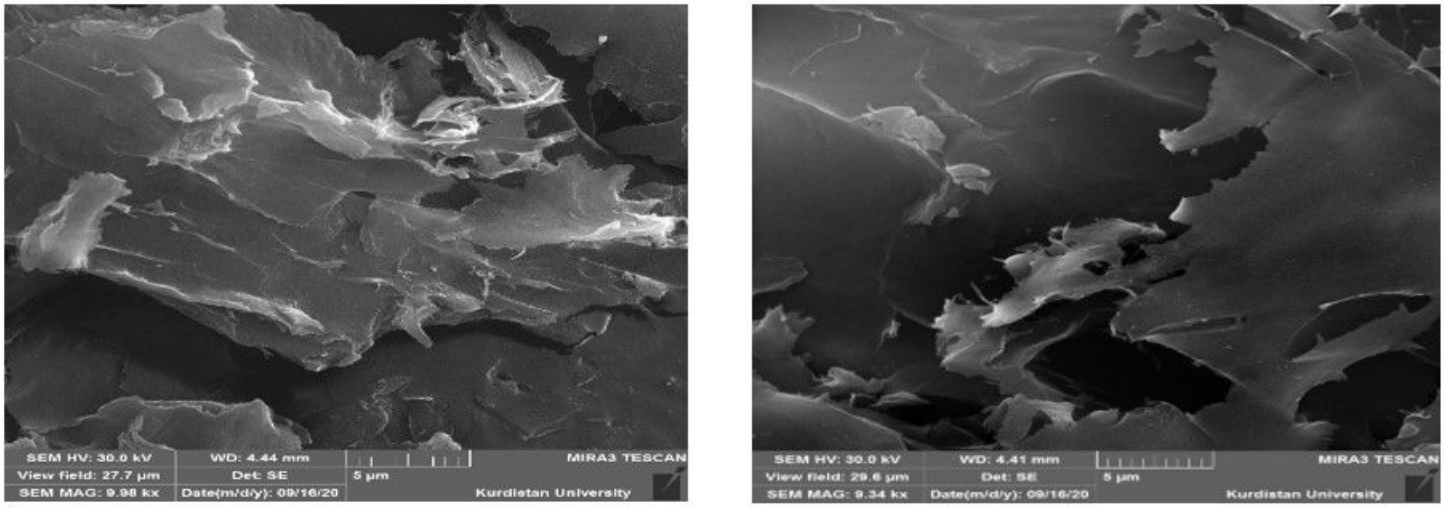

Figure 2

SEM images for CNC (a) CNC-Ser (b)

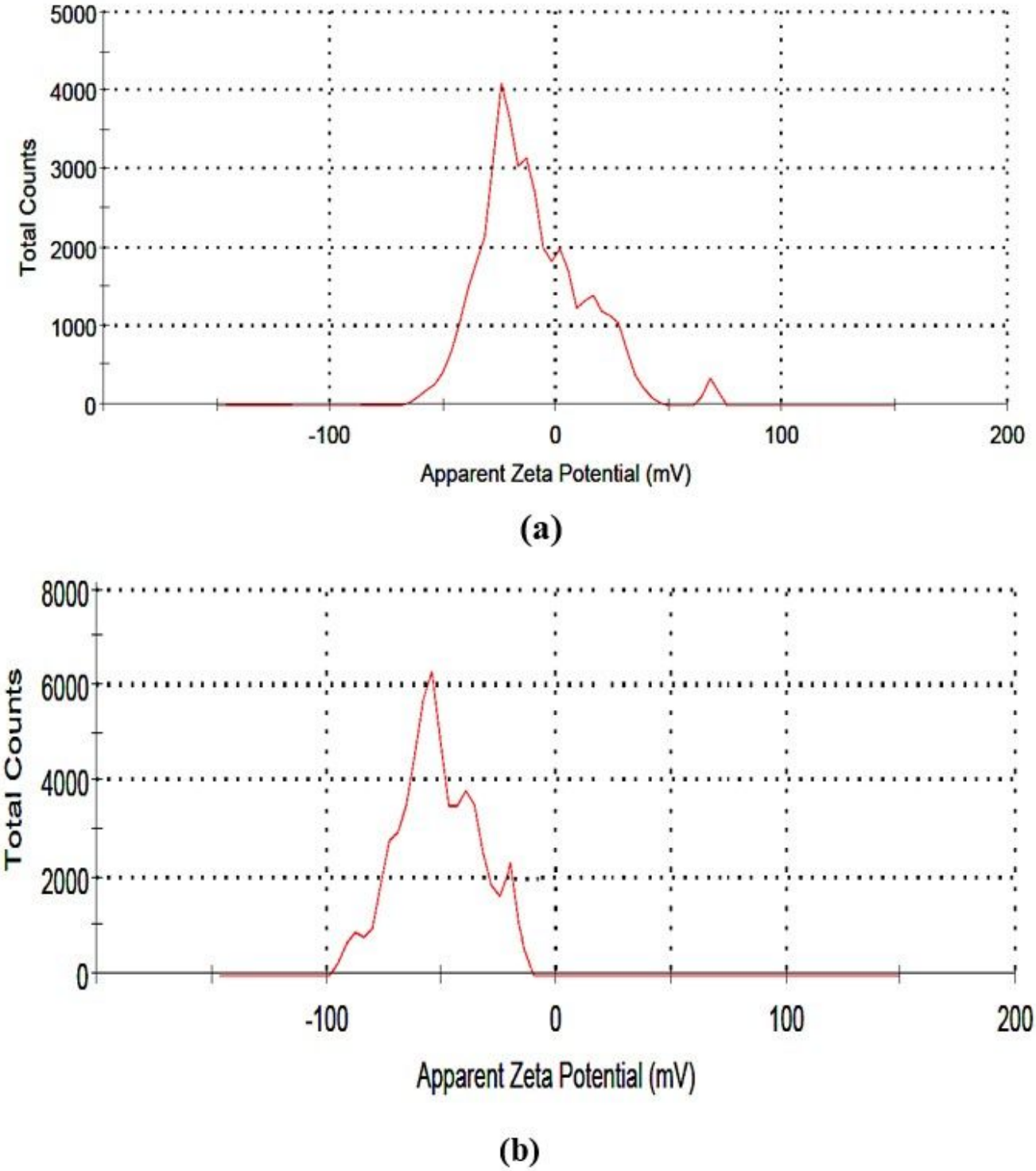

Figure 3

Zeta potential of CNC (a) and CNC-Ser (b)

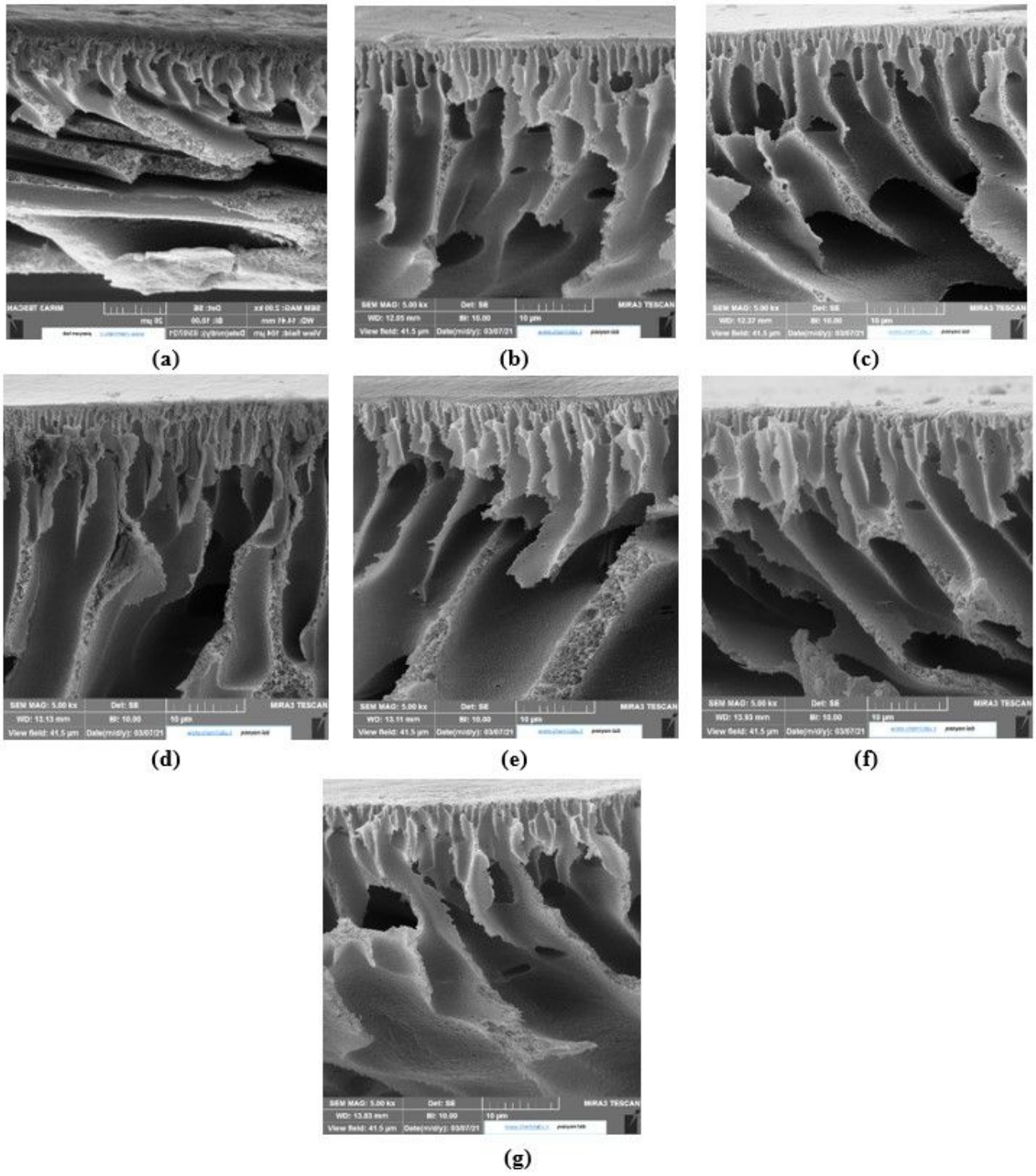

Figure 4

SEM images of the fabricated membranes. M1: bare membrane (a), M2: 0.1wt % CNC (b), M3: 0.5 CNC (c), M4: 1wt % CNC (d), M5: 0.1wt % CNC-Ser (e), M6: 0.5wt% CNC-Ser (f), M7: 1wt% CNC-Ser (g).

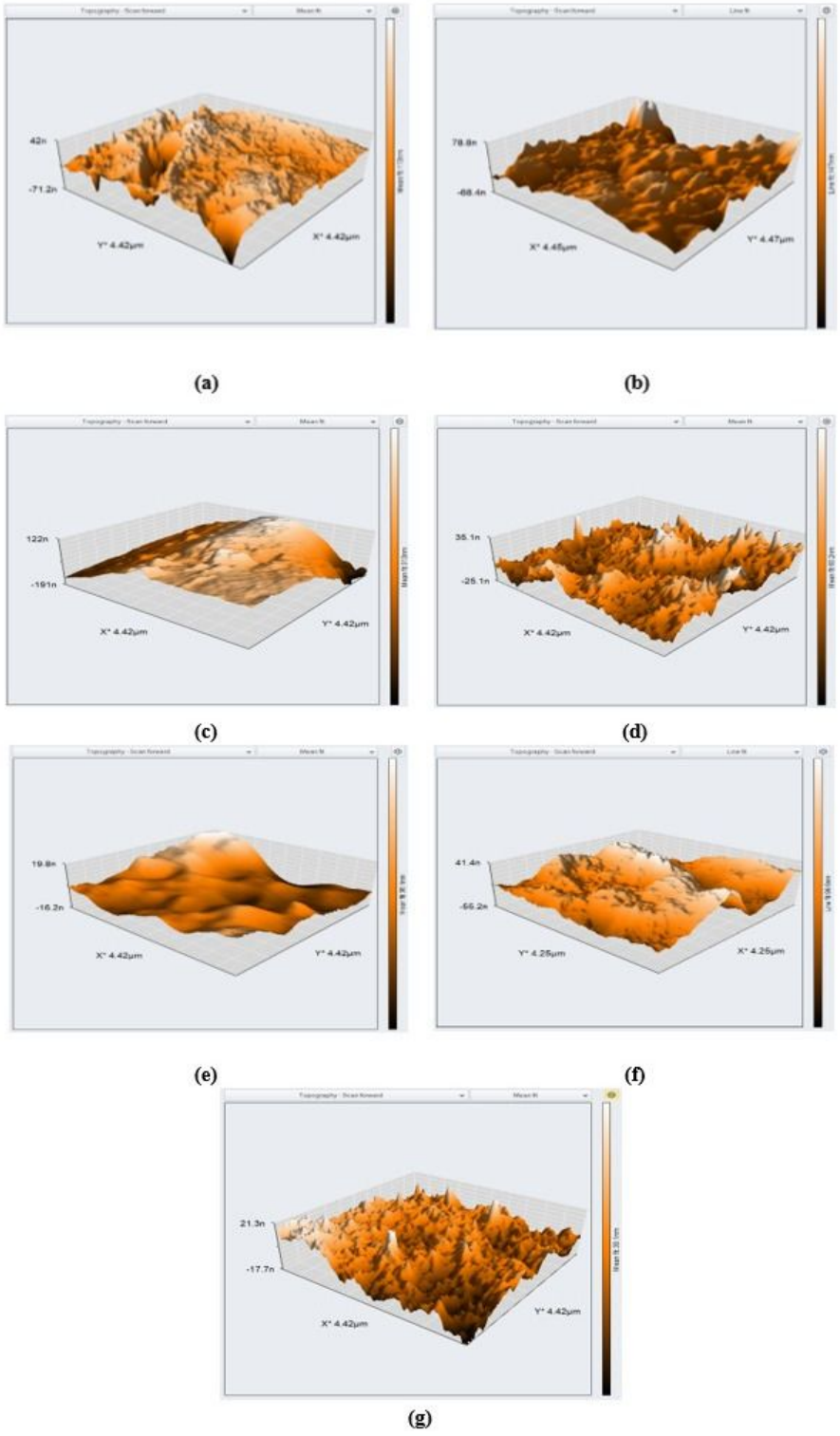

Figure 5

AFM images of (a) M1 bare membrane, (b) M2 0.1wt % CNC, (c) M3 0.5wt % CNC, (d) M4 1wt % CNC, (e) M5: 0.1wt % CNC-Ser, (f) M6: 0.5 wt% CNC-Ser, (g) M7: 1wt% CNC-Ser

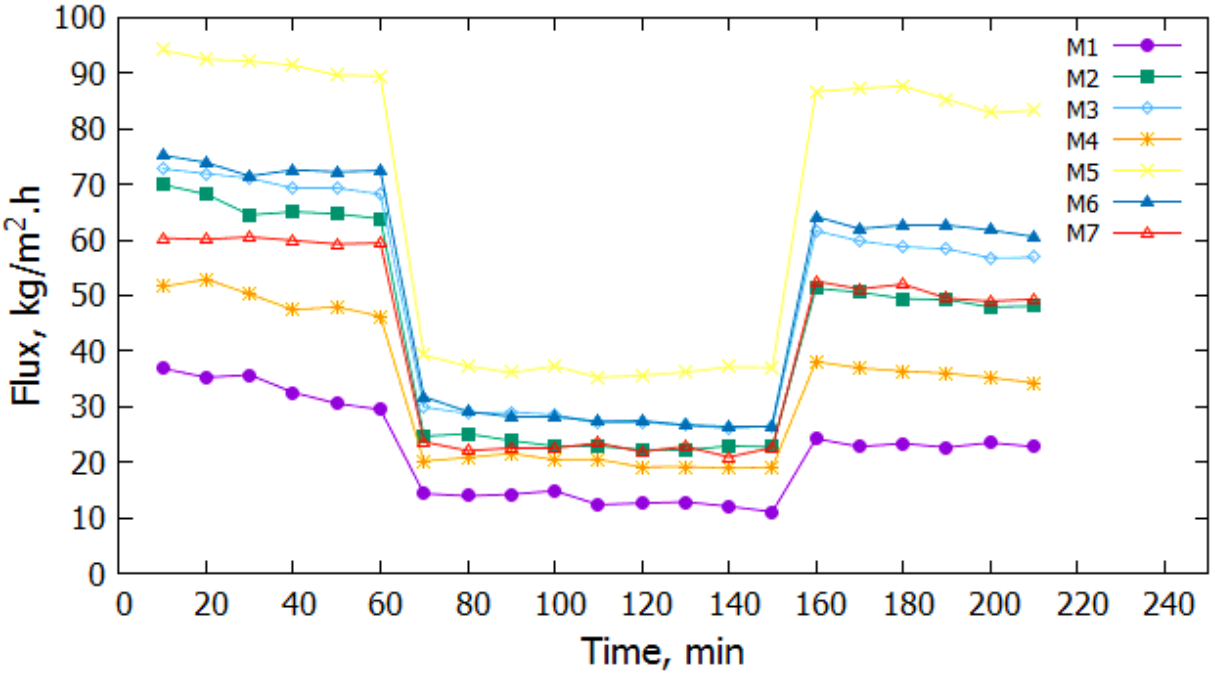

Figure 6

Three frequent step experiment: (i) distilled water, (ii) 1000 ppm milk powder solution, and (iii) distilled water filtration.

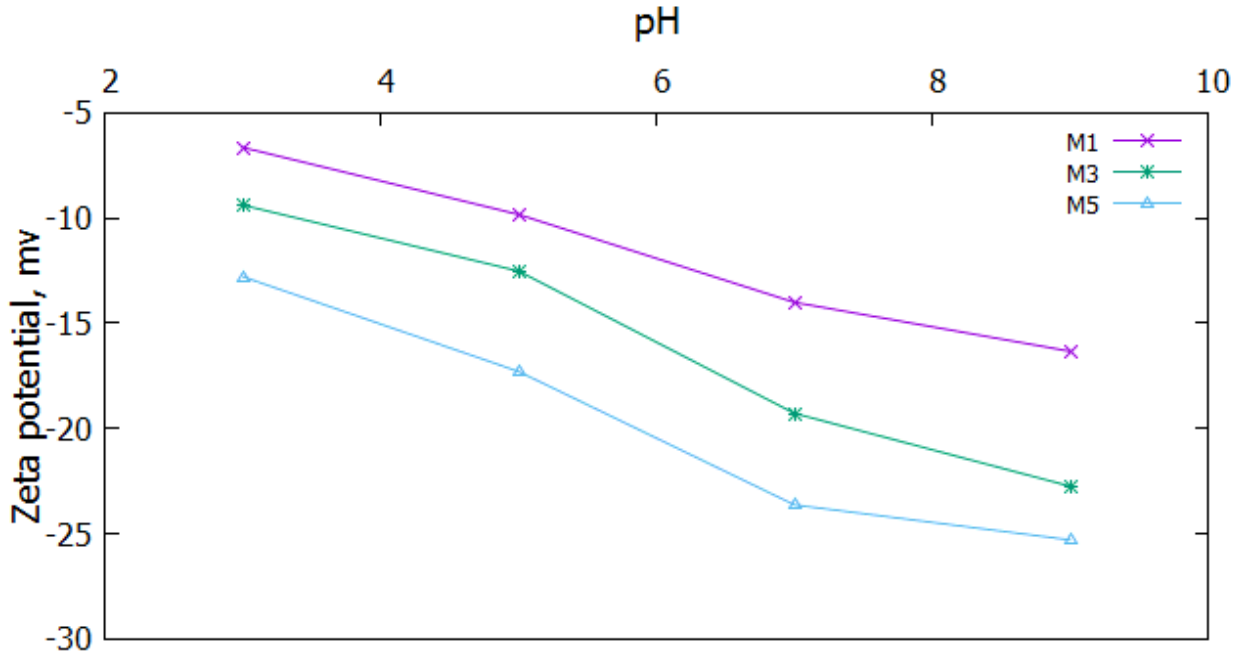

Figure 7

Surface zeta potential of membranes M1, M3, and M5.

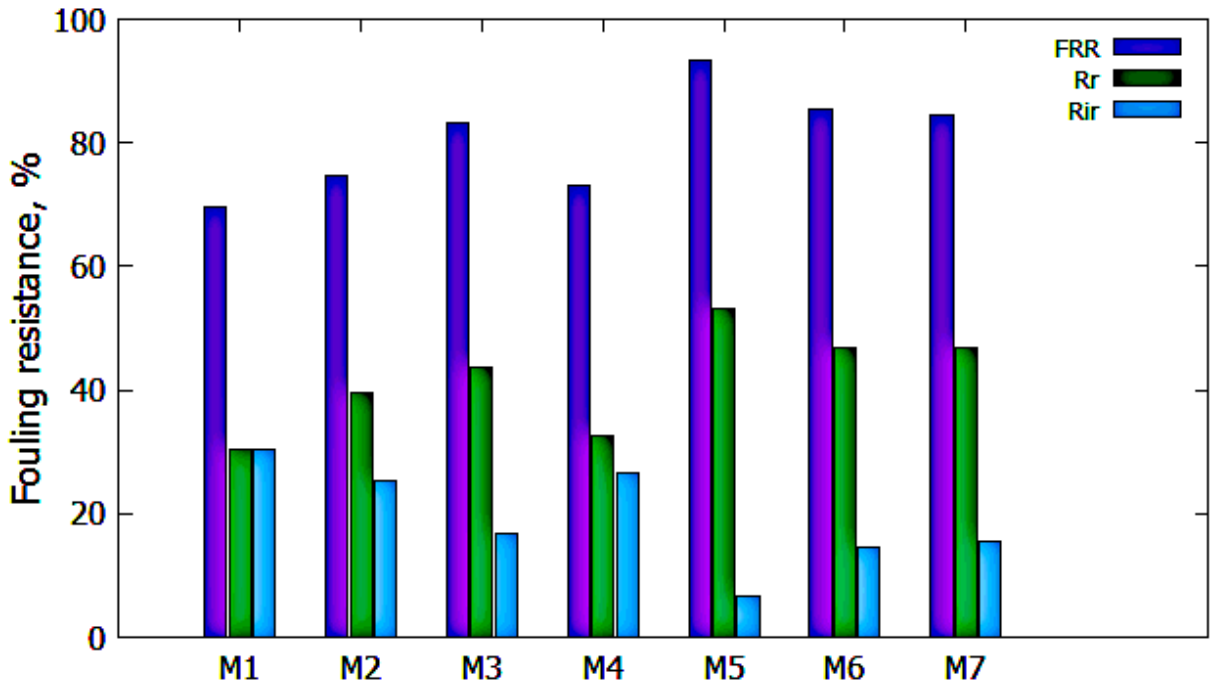

Figure 8

FRR, reversible (Rr) and irreversible (Rir) fouling resistance results of the fabricated membranes.

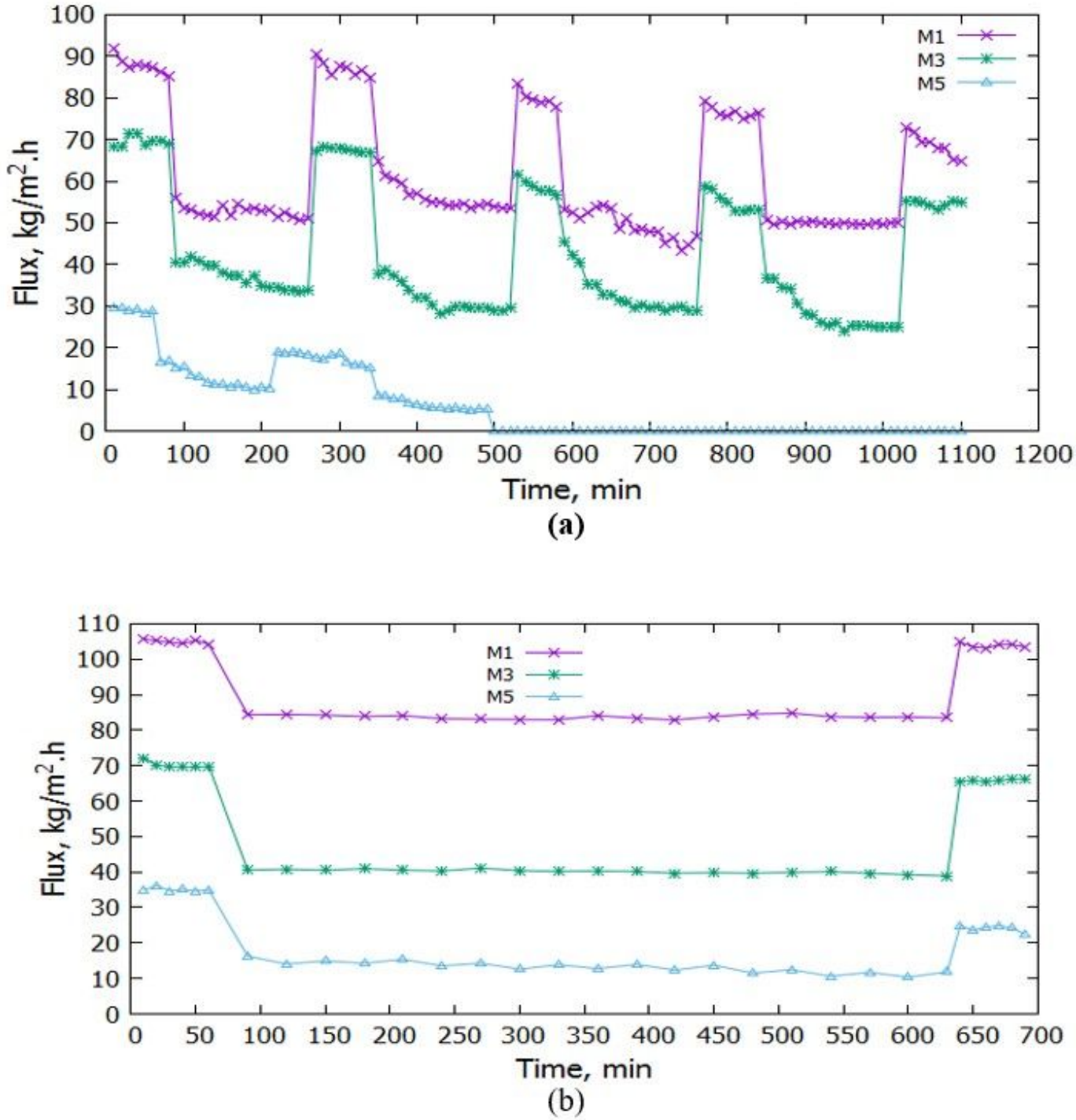

Figure 9

Long-term filtration for unmodified and optimal modified membranes in dead-end (a) and cross-flow (b) setup